Tellus (1997), 49B, 38–55
Printed in UK – all rights reserved

TELLUS
ISSN 0280–6509

Model study of the influence of cross-tropopause O_3 transports on tropospheric O_3 levels

By GEERT-JAN ROELOFS* and JOS LELIEVELD, *Institute for Marine and Atmospheric research Utrecht (IMAU), Princetonplein 5, 3584 CC Utrecht, The Netherlands*

(Manuscript received 9 February 1996; in final form 24 June 1996)

ABSTRACT

Cross-tropopause transport of O_3 is a significant factor in the tropospheric budget and distribution of O_3. Nevertheless, the distribution in the troposphere of O_3 that originates from the stratosphere is uncertain. We study this with a chemistry — general circulation model with relatively high spatial and temporal resolution. The model simulates background tropospheric CH_4-CO-NO_x-HO_x photochemistry, and includes a tracer for stratospheric O_3. Since this tracer is not photochemically produced in the troposphere but only destroyed, comparing its budget and distribution with that of total tropospheric O_3 yields an estimate of the contribution of the stratospheric O_3 source in the troposphere. Model results suggest that transport from the stratosphere and net photochemical formation in the troposphere, considering present-day emissions, are of comparable magnitude. The model predicts efficient transport of upper tropospheric O_3-rich air to the surface by large-scale subsidence in the subtropics and by synoptic disturbances in the NH middle and high latitudes. O_3 from the stratosphere contributes significantly to surface O_3 in winter and spring when the photochemical lifetime of O_3 is relatively long. In summer and in the tropics, little O_3 from the stratosphere reaches the surface due to strong photochemical destruction, so that surface O_3 is largely determined by photochemical production. Photochemically produced O_3 maximizes in the free troposphere where the O_3 surface warming efficiency is higher compared to the boundary layer.

1. Introduction

An important source of O_3 in the troposphere is downward transport from the stratosphere through tropopause foldings associated with large-scale cyclogenesis, cut-off lows, and quasi-adiabatic transports along isentropic surfaces (Danielsen, 1968; Vaughan, 1988; Holton et al., 1996). Stratosphere-troposphere exchange (STE) of O_3 co-determines the distribution of O_3 in the troposphere, and knowledge of its influence on tropospheric O_3 levels is necessary to assess the climate effects of O_3 perturbations due to human activities (Fishman et al., 1979; Ramanathan et al., 1987).

* Corresponding author.

Although the important exchange mechanisms have been identified, budgets of the annual and global cross-tropopause transport of O_3 are still highly uncertain. General circulation model (GCM) calculations yield cross-tropopause O_3 fluxes between 475 and 650 Tg O_3 yr^{-1} (Mahlman et al., 1980; Gidel and Shapiro, 1980; Levy et al., 1985). Based on correlations between N_2O and O_3, potential vorticity (PV) and O_3, and ^{90}Sr and O_3, ozone fluxes have been calculated ranging from 200 to 870 Tg O_3 yr^{-1} globally (Murphy and Fahey, 1994), and 500 Tg O_3 yr^{-1} for the northern hemisphere (Danielsen and Mohnen, 1977). Ebel et al. (1993) used a regional model to assess the cross-tropopause transport of O_3 for a combined tropopause folding and cut-off cyclone event, and extrapolated an O_3 flux of 770–960 Tg yr^{-1} for the northern hemisphere.

The 2nd source of tropospheric O_3 is photochemical production as a result of NO_x, CO, CH_4, and higher hydrocarbon emissions (Crutzen, 1995). Tropospheric O_3 budget calculations with two- or three-dimensional global transport chemistry models yield global cross-tropopause fluxes between 408 and 1077 Tg O_3 yr^{-1}, net photochemical production fluxes between 216 and 1404 Tg O_3 yr^{-1}, and dry deposition fluxes between 612 and 1937 Tg O_3 yr^{-1} (WMO, 1995). These global budget terms, however, do not indicate how the stratospheric O_3 source contributes to the tropospheric O_3 distribution.

To investigate this, Levy et al. (1985) prescribed O_3 mixing ratios at the 10 hPa level of a GCM, and simulated downward O_3 transport and destruction at the earth's surface. They concluded that observed vertical profiles and surface seasonal cycles of O_3 are fairly well reproduced by only considering a stratospheric source for tropospheric O_3. However, the lack of a tropospheric photochemistry representation in the model caused too high O_3 levels at high latitudes in the northern hemisphere, and spring maxima and autumn minima instead of the observed summer maxima and winter minima at NH middle and high latitudes. Follows and Austin (1992) used a two-dimensional NH tropospheric model that included photochemistry and explicitly accounted for O_3 of stratospheric origin. They found that stratospheric O_3 contributed less than 5% to surface O_3, although at 300 hPa the contribution was significant. Holton and Lelieveld (1996), using a simplified three-dimensional global chemistry/transport model, reached a similar conclusion. Thus, there appear to be large discrepancies among different studies regarding the importance of STE for tropospheric O_3.

In the present study we use a chemistry — GCM, described in Roelofs and Lelieveld (1995), to analyse tropospheric O_3 in terms of contributions from STE and photochemical production in the troposphere. In the present version, the model calculates background CH_4-CO-NO_x-HO_x tropospheric chemistry and global meteorology on a relatively high spatial and temporal resolution ($3.75° \times 3.75°$ and 1800 s, respectively). At this resolution the GCM realistically simulates synoptic disturbances such as extratropical cyclones. This is important since associated downward flows carry upper tropospheric O_3, originating from the stratosphere, to the surface, where its lifetime is considerably shorter. Thus, the representation of vertical transport is expected to be more realistic in our model than in that of Follows and Austin (1992) who used a parameterization based on eddy diffusion, and of Holton and Lelieveld (1996) who used monthly averaged meteorology.

Following the method of Follows and Austin (1992), we have included a tracer for stratospheric O_3 in the model (referred to as O_3s). This tracer is treated in the same way as O_3, except that the reactions involving O_3s in the troposphere are only those that destroy O_3. Thus, its only source in the troposphere is cross-tropopause transport. A brief description of the coupled chemistry — GCM will be given in Section 2. Section 3 presents calculated budgets and distributions of the different O_3 "types" in the troposphere. Section 4 presents the conclusions.

2. Model description

2.1. General

The general circulation model used in this study is the European Center Hamburg Model, version 4 (ECHAM4). In the T30 mode, which is used in this study, the horizontal resolution is approximately $3.75° \times 3.75°$ and the time resolution is 1800 s. The model uses 19 vertical layers in a hybrid σ-p- coordinate system, from the surface to 10 hPa. Average pressure levels relevant for the troposphere and lower stratosphere are 990, 970, 950, 900, 840, 760, 670, 580, 490, 400, 320, 250, 190, 140, 100 and 75 hPa, referring to approximate mid-layer altitudes of 0.03, 0.14, 0.38, 0.78, 1.4, 2.1, 3.1, 4.2, 5.6, 7.0, 8.6, 10.2, 11.9, 13.8, 15.9 and 18.0 km above the surface. Tracer transport is calculated using a semi-Lagrangian advection scheme (Rasch and Williamson, 1990; Feichter et al., 1996). Additional vertical transports are included through parameterizations for vertical diffusion and convection (Roeckner et al., 1992; Tiedtke, 1989). An elaborate description of ECHAM and the simulated climate can be found in Roeckner et al. (1992, 1995), Boer et al. (1992), and Haskins et al. (1995). The climate model has previously been used for tracer transport studies (Feichter et al., 1991; Brost et al., 1991) and a simulation of the global sulfur cycle (Feichter et al., 1996).

The GCM is coupled to a tropospheric chemistry model, that considers background CH_4-CO-NO_x-HO_x chemistry, emissions of NO and CO, dry deposition of O_3, NO_2, HNO_3, and H_2O_2, and wet deposition of HNO_3 and H_2O_2. A description and analysis of the general circulation — chemistry model is given in Roelofs and Lelieveld (1995). The coupled model gives a realistic representation of the seasonal variabilities of the O_3 photochemical production and of O_3 transport from the stratosphere. Calculated O_3 profiles and surface concentrations for remote tropical and mid-latitudinal sites agree well with observations. The model underestimates O_3 concentrations at the poles and in relatively polluted regions. The latter is due to the neglect of higher hydrocarbon chemistry.

In the latest version of the model we use more recent estimates for the NO emission distributions. Anthropogenic NO emissions (21 Tg N yr^{-1}) are distributed according to Benkovitz et al. (1996), soil NO emissions (5.5 Tg N yr^{-1}) according to Yienger and Levy (1995), and biomass burning NO emissions (6 Tg N yr^{-1}) according to Hao and Liu (1994). The distribution of NO emissions by lightning (4 Tg N yr^{-1}) is calculated on-line based on the calculated cloud top heights for convective clouds (Price and Rind, 1992). The total NO source amounts to 36.5 Tg N yr^{-1}. We have included the dry deposition parameterization for O_3, NO_x, and HNO_3 of Ganzeveld and Lelieveld (1995), that derives aerodynamic and stomatal resistances directly from parameters calculated by ECHAM4. Further, a new definition for the tropopause is adopted (see Subsection 2.2). In this study we use the results of a two-year simulation. The modifications have altered the tropospheric O_3 budget compared to the previous model version, and the agreement between the calculated and observed seasonality of O_3 surface concentration has significantly improved, as will be discussed in Section 3.

2.2. *Tropopause and stratospheric O_3*

Since the chemistry in the model is representative for background tropospheric conditions, stratospheric O_3 concentrations are prescribed between 1 to 2 model layers above the tropopause up to 10 hPa, the top level of the GCM, using the results of a 2D troposphere-stratosphere chemical model (Brühl and Crutzen, 1988). In the previous version the tropopause height was determined on the basis of the potential temperature lapse rate, in the present version a dynamical tropopause is determined poleward of 20° latitude using the calculated potential vorticity (PV). The 3.5 PV-unit (3.5 10^{-6} K $m^2 kg^{-1} s^{-1}$) level is assumed to designate the extratropical tropopause (Hoerling et al., 1993). Note that our results do not change significantly by using a 2 PV-unit tropopause definition, as recommended by Appenzeller et al. (1996), which is probably due to the relatively coarse resolution of the model in the tropopause region (1.5 to 2 km). Towards the equator PV vanishes, and a temperature lapse rate of -2 K km^{-1} is applied to mark the boundary between the troposphere and the stratosphere.

2.3. *Tracer of stratospheric O_3 in the troposphere*

Apart from O_3, the model considers a tracer for O_3 that originates from the stratosphere, referred to as O_3s. In the stratosphere O_3s is treated in the same way as O_3. It is transported from the stratosphere into the troposphere along with the calculated air motions. Photochemical production of O_3 takes place through the reactions:

$$NO + HO_2 \rightarrow NO_2 + OH \qquad \text{R1}$$

$$NO + CH_3O_2 \rightarrow NO_2 + CH_3O \qquad \text{R2}$$

$$NO_2 + h\nu \rightarrow NO + O(^3P) \qquad (\lambda < 430\ \text{nm}) \quad \text{R3}$$

$$O(^3P) + O_2 + M \rightarrow O_3 + M \qquad \text{R4}$$

These reactions are omitted for O_3s in the troposphere. However, O_3s is destroyed in the same way as O_3 by:

$$O_3 + OH \rightarrow O_2 + HO_2 \qquad \text{R5}$$

$$O_3 + HO_2 \rightarrow 2O_2 + OH \qquad \text{R6}$$

$$O_3 + h\nu \rightarrow O(^1D) + O_2 \qquad (\lambda < 315\ \text{nm}) \quad \text{R7}$$

$$O(^1D) + H_2O \rightarrow 2OH \qquad \text{R8}$$

Part of the $O(^1D)$ formed in R7 recombines to form O_3s through R4 after the quenching reaction:

$$O(^1D) + M \rightarrow O(^3P) + M \qquad \text{R9}$$

The reaction sequence R7, R9 and R4 does therefore not result in loss of O_3s. The total chemical loss rate of O_3s in the troposphere is given by:

$$L_{O_3s} = k_5[OH] + k_6[HO_2] + \frac{J_7 k_8 [H_2O]}{k_6[M] + k_8[H_2O]},$$

in which k- and J-values represent reaction rates and photodissociation coefficients, respectively, for reactions R5-R8, and the square brackets indicate concentrations. The loss term is part of the Eulerian Backward Iterative (EBI) integration scheme for the gaseous chemical reactions (Roelofs and Lelieveld, 1995). Dry deposition of O_3s is calculated as that of O_3.

The difference between calculated budgets and concentrations of O_3 and O_3s gives an indication of the O_3 amount that originates within the troposphere. This O_3 "type" (referred to as O_3t) represents O_3 that is photochemically produced from natural and anthropogenic emissions of O_3 precursors. It is chemically produced through reactions R1 and R2, and destroyed through R5, R6, and R8. Apart from R5, R6, and R8, two reactions involving NO_3 and N_2O_5 lead to additional destruction of O_3. Yearly averaged, their global significance in terms of O_3 destruction is of the order of a few percent. In our model they affect O_3t but not O_3s.

3. Results

3.1. *Tropospheric O_3 budget*

Table 1 shows the calculated budget of O_3, O_3s, and O_3t in the troposphere. The budget terms are: transport into the troposphere, the net result of chemical production and destruction, dry deposition, and the tropospheric content. The transport terms reflect the net changes in tropospheric O_3 content of the hemispheres due to STE and to interhemispheric exchange. The latter two terms cannot be calculated separately. However, in the equatorial region, especially in the intertropical convergence zone (ITCZ) near the surface, the chemical lifetime of tropospheric O_3 is only of the order of a few days due to high insolation and

Table 1. *Budgets of tropospheric O_3, O_3s, and O_3t*

		O_3		O_3s		O_3t	
		NH	SH	NH	SH	NH	SH
Transport into troposphere	DJF	80	34	132	93	−51	−60
	MAM	74	77	157	108	−83	−30
	JJA	34	99	131	116	−97	−17
	SON	34	26	101	92	−67	−66
	annual	*223*	*236*	*521*	*409*	*−298*	*−173*
	ann. global	*459*		*930*		*471*	
Chemical formation	DJF	3	−21	−87	−90	90	69
	MAM	47	−22	−151	−80	198	57
	JJA	59	−28	−136	−84	195	56
	SON	45	−9	−73	−114	118	105
	annual	*155*	*−80*	*−446*	*−368*	*601*	*288*
	ann. global	*75*		*−814*		*888*	
Dry deposition	DJF	−71	−30	−23	−4	−47	−25
	MAM	−107	−34	−23	−10	−84	−25
	JJA	−114	−48	−15	−18	−99	−30
	SON	−85	−46	−16	−12	−69	−34
	annual	*−377*	*−158*	*−77*	*−43*	*−300*	*−114*
	ann. global	*−534*		*−120*		*−414*	
Tropospheric content	DJF	145	102	68	37	77	65
	MAM	169	107	70	48	99	59
	JJA	153	135	48	69	105	66
	SON	141	133	45	56	96	77
	annual	*152*	*119*	*58*	*52*	*94*	*67*
	ann. global	*271*		*110*		*161*	

Transport, chemical formation and dry deposition in Tg O_3 per 3 months or Tg O_3 per year, tropospheric content in Tg O_3.

high water vapor concentrations. The ITCZ is a relatively strong sink for tropospheric O_3 which causes interhemispheric transport of O_3 to be relatively small compared to other sources of tropospheric O_3. Therefore, horizontal transports are not explicitly considered in Table 1.

Compared to the previous version of the model (Roelofs and Lelieveld, 1995) the annual global dry deposition flux of O_3 has decreased by about 205 Tg due to the direct coupling of dry deposition of O_3, NO_x, and HNO_3 with the calculated boundary layer meteorology and surface characteristics. In addition, the net downward transport of O_3 into the troposphere has decreased by 115 Tg O_3 yr^{-1}, which is largely due to the use of a different model version at higher resolution. The net chemical formation of O_3 has decreased by approximately 95 Tg yr^{-1}, resulting in a balance between sources and sinks. The net formation is the result of photochemical destruction of O_3 transported from the stratosphere (O_3s) and photochemical production of O_3 in the troposphere (O_3t). The gross photochemical production of O_3, mainly the result of reactions R1 and R2, has increased compared with the previous version from 3190 Tg O_3 yr^{-1} to 3425 Tg O_3 yr^{-1}. Combined with the lower dry deposition flux this has resulted in an increase of the annually averaged tropospheric O_3 content to 271 Tg.

The net flux of O_3 into the troposphere is the result of a downward flux of stratospheric O_3 and an upward flux of O_3 that has been photochemically produced in the troposphere, with a ratio of about 2:1. The relatively large up and down fluxes of O_3 are a consequence of two-way isentropic exchange between the upper troposphere and lowermost stratosphere in the extratropics (Hoerling et al., 1993; Holton et al., 1996). In addition, some tropospheric O_3 is transported upward into the stratosphere in the tropics by convection.

Considering the concentrations of O_3s and O_3t near the tropopause (shown in Figs. 1, 2, discussed in Subsection 3.2), the ratio between the downward O_3s and upward O_3t fluxes of 2:1 appears rather low. However, in winter and spring downward cross-tropopause transports of O_3s are relatively large while O_3 lifetimes in the troposphere are relatively long. Once in the troposphere, O_3s is partly transported back from the upper troposphere to the stratosphere. The gross downward O_3s flux may therefore exceed the flux listed in Table 1 significantly. On the other hand, upward O_3t fluxes peak in the NH summer and autumn and the SH spring (the biomass burning season) and summer. Calculated upward/downward ratios are then up to 4:3. During these seasons photochemical destruction of O_3 in the stratosphere is relatively efficient, and the return flux of O_3t back into the troposphere is probably relatively small compared to the upward flux. Nevertheless, calculated upward and downward O_3 fluxes are likely to be overestimated to some extent as a result of numerical diffusion associated with the relatively coarse vertical resolution of the model around the tropopause. Reducing numerical diffusion by application of a finer vertical resolution may decrease the downward O_3s and upward O_3t fluxes and increase the corresponding ratio.

Annually, about 30% more O_3s enters the troposphere in the NH than in the SH. Because upward transport of O_3t is also larger in the NH, the net O_3 downward transport is about equal in both hemispheres. Compared to the previous model version, where net O_3 transport in the NH exceeded that in the SH by approximately 50%, STE of O_3 in the NH has decreased. This is due to the reduced vertical transport efficiencies in the higher resolution model and to the lower dry deposition flux of O_3, which results in an increased O_3t content, and subsequently an increased upward transport of O_3t into the lower stratosphere.

The cross tropopause transport of O_3s follows a seasonal cycle, with a maximum in the spring in the NH, and in the winter in the SH. The tropospheric content and the dry deposition of O_3s also maximize in these seasons. Photochemical destruction peaks in spring when O_3s, that has accumulated during the winter, is subject to increasing insolation, temperature, and humidity. On average, 13% of the O_3s that enters the troposphere reaches the surface and is removed by dry deposition, the rest is photochemically destroyed. In the NH, photochemical production, dry deposition and the tropospheric content of O_3t maximize in spring and summer. The flux of O_3t from the troposphere into the lowermost stratosphere is largest in the summer season, despite the fact that cross-tropopause transport of air is at minimum. High O_3t concentrations in the NH summer result

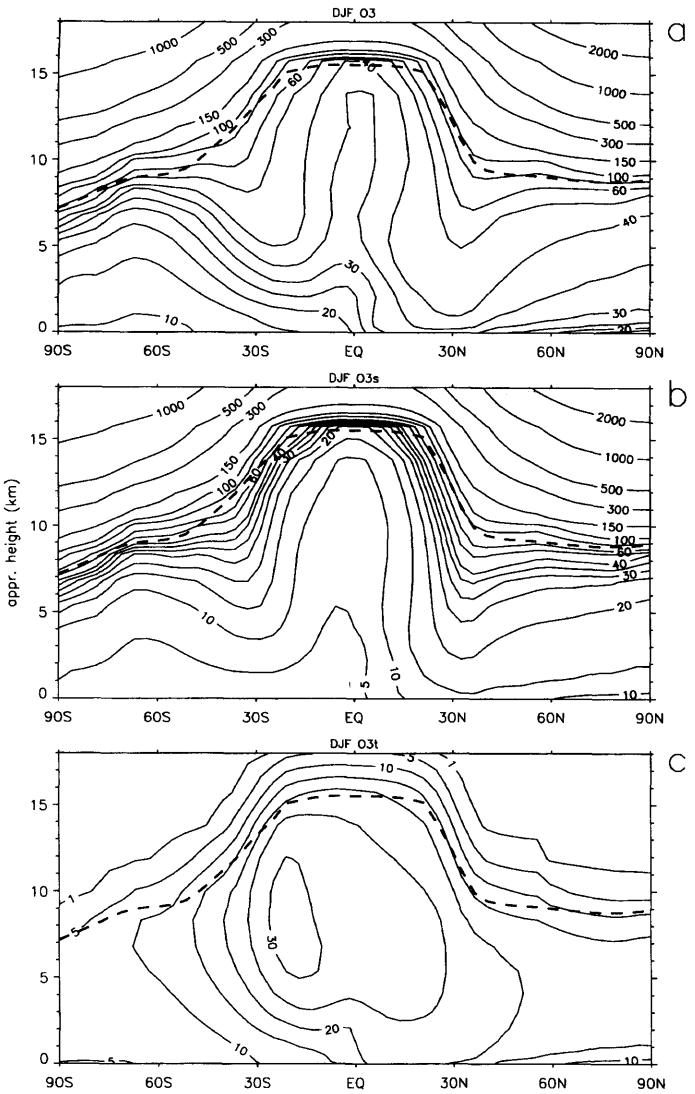

Fig. 1. Zonally averaged mixing ratios (ppbv) of (a) O_3, (b) O_3 originating from the stratosphere (O_3s), and (c) O_3 from photochemical production in the troposphere (O_3t), for December, January, February (DJF). Contour lines at 1, 5, 10, 15, 20, 25, 30, 35, 40, 50, 60, 80, 100, 150, 300, 500, 1000 and 2000 ppbv. The dashed line indicates the tropopause.

predominantly from industrial emissions which occur at middle and high latitudes, whereas transport of O_3t to tropical regions is relatively inefficient because of strong chemical destruction. This suggests that during summer most upward cross-tropopause transport of O_3t takes place in the extratropics. This appears to be relevant for evaluations of the radiative forcing of climate by anthropogenic activities, because the summertime tropopause region is particularly sensitive to radiative perturbations by changing O_3 (Ramanathan et al., 1987). In the SH, O_3t burdens are largest during spring, coinciding with the biomass burning maximum.

The model results indicate that the 2 sources of ozone in the troposphere, i.e., net photochemical

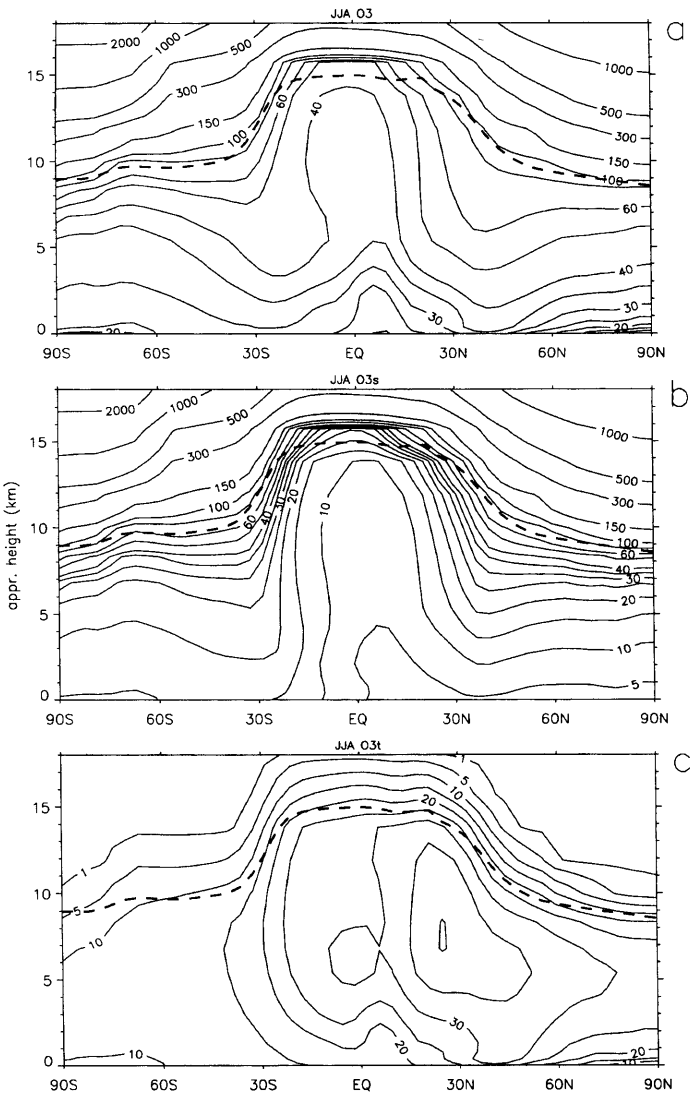

Fig. 2. As Fig. 1, but for June, July, August (JJA).

production of O_3t and transport of O_3s from the stratosphere, are of comparable magnitude. However, the gross photochemical O_3 production is almost a factor of 4 larger. In terms of tropospheric content, we calculate that the summer and winter contributions of O_3s are approximately 30 and 45% in the NH, and 35 and 50% in the SH, with a global annual average of approximately 40%. The average lifetime of O_3s in the troposphere ranges from approximately 30 days in the summer hemisphere to 50 days in the winter hemisphere.

3.2. *Distribution of O_3, O_3s and O_3t in the troposphere*

Figs. 1 and 2 show the zonally averaged mixing ratios of O_3, O_3s, and O_3t for December, January, and February (DJF) and for June, July, and August (JJA). The different distributions of O_3s

and O_3t can be clearly discerned. The simulated tropopause height, seasonally and zonally averaged, is shown by the dashed line. Tropospheric concentrations of O_3s are highest near the tropopause, and decrease with altitude as O_3s is destroyed by photochemical processes and surface deposition. Between 20° and 50° latitude the concentrations of O_3s are relatively high in the middle troposphere. In the subtropics, O_3s is transported downward through the tropopause breaks. Large-scale subsidence at these latitudes further transports O_3 down to the surface. In the middle and high latitudes O_3s amounts are larger in winter than in summer (see also Table 1). Between 20°S and 20°N, concentrations of O_3s are relatively small throughout the year, particularly in the ITCZ. In the tropical troposphere, high insolation and high water vapor concentrations lead to efficient chemical destruction of O_3 through reactions R7 and R8, so that the O_3 lifetime near the surface is less than a week.

In JJA, photochemical production of O_3t is efficient in the middle and high latitudes of the NH due to the combination of strong photochemical activity, anthropogenic NO_x-emissions, and convective transports of trace gases out of the polluted boundary layer. Near the surface the concentrations are lower as a result of dry deposition. In the SH summer, DJF, significant production of O_3t occurs between the equator and 30° S, mostly due to emissions from the African and South American continents. Convection transports part of the emitted NO_x into the free troposphere where it leads to O_3 production. NO produced by lightning at higher altitudes further contributes to this. In the SH, however, surface emissions are strongest between August and November, associated with biomass burning. These produce the highest O_3 concentrations throughout the year in these regions, as will be discussed below.

The contributions of O_3s and O_3t to tropospheric O_3 are further illustrated in Fig. 3. It shows monthly variations of zonally averaged mixing ratios of O_3, O_3s, and O_3t at the surface. In the NH, the surface concentration of O_3 has a distinct maximum during spring. Such a maximum is often observed in locations in the NH that are not directly affected by photochemical pollution, such as Mace Head and Izaña (Oltmans and Levy, 1994). In middle latitudes, relatively high concentrations of O_3 persist until the autumn. In the NH, surface concentrations of the stratospheric component, O_3s, maximize in winter and early spring, they are lowest in the summer (< 5 ppbv), and increase again in the autumn. On the other hand, the zonally averaged photochemical component, O_3t, is smallest during winter and has a maximum in late spring and early summer. In the SH, O_3 maximizes in winter, influenced mostly by the stratospheric influx of O_3. Highest concentrations of O_3t in the SH are found between 20°S and the equator between August and November as a result of biomass burning emissions.

Fig. 4 shows the monthly variations of zonally averaged O_3, O_3s, and O_3t mixing ratios at the 500 hPa level. For total O_3, the seasonality at 500 hPa is somewhat different than at the surface. In the NH, the spring peak shifts slightly towards the summer, whereas in the SH a distinct maximum appears between 30° and the equator during SON. This is associated with the emissions of O_3 precursors, which are transported upward by convection to altitudes where O_3 lifetimes are several times longer that at the surface. Thus, although in the boundary layer NO_x levels and thus O_3 production rates are higher, at the same time photochemical destruction and surface deposition efficiently remove O_3. Consequently, O_3t mixing ratios are up to 100% higher at 500 hPa than at the surface around the globe. The seasonality of O_3s at 500 hPa is very similar to that at the surface, but the mixing ratios are higher. Tropical O_3s concentrations are relatively low throughout the year both at the surface and at 500 hPa. The area of low O_3s shifts from south of the equator in DJF to north of the equator in JJA, following the movement of the ITCZ.

Fig. 5 shows the calculated monthly averaged concentrations of O_3, O_3s, and O_3t for model grids in which the measurement sites Mace Head, Payerne, Mauna Loa, Samoa, Cape Point, and Cape Grim are located. Open squares denote observed O_3 levels, adopted from Oltmans and Levy (1994) and, for Payerne, from the World Ozone Data Centre (WODC). The calculated mixing ratios pertain to the surface layer ($\sim$30 m above the surface), except for Payerne (altitude: 490 m) and Mauna Loa (3400 m) where model layers closest to the height of the measurement sites have been chosen. Payerne is a continental site with relatively polluted conditions, the other

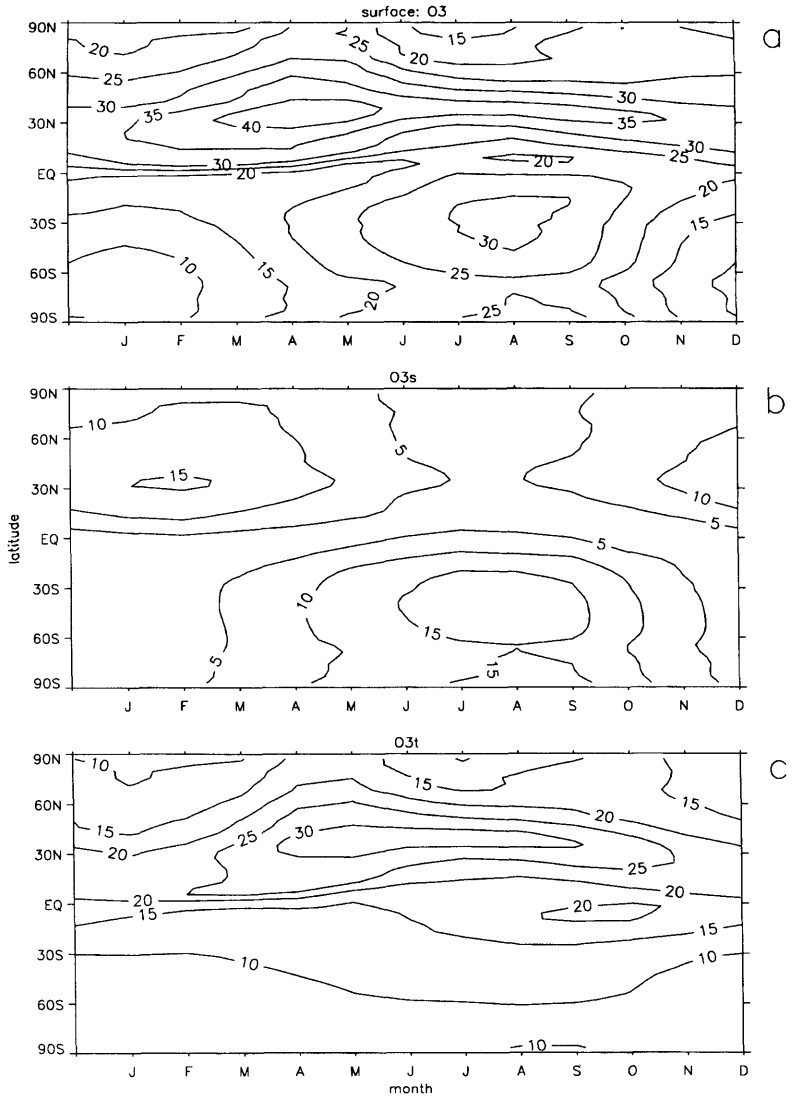

Fig. 3. Monthly variation of zonally averaged mixing ratios (ppbv) for (a) total O_3, (b) O_3 originating from the stratosphere (O_3s), and (c) O_3 originating from photochemical production in the troposphere (O_3t), at the surface.

locations are remote and represent relatively clean, background conditions. Compared to Roelofs and Lelieveld (1995) the seasonality and absolute concentrations of O_3 at the surface have significantly improved for all sites (Payerne was not part of the previous analysis). The improvements are mainly due to the higher model resolution which results in a better representation of transport processes, and to the new dry deposition parameterization for O_3, NO_x, and HNO_3, which refines the consistency between the chemistry and surface removal calculations. At Payerne, O_3 concentrations are somewhat overestimated in winter and underestimated in summer, although the observed winter minimum and summer maximum are reproduced well. The comparison between modelled and observed O_3 is also discussed in Roelofs and Lelieveld (1995) and Dentener et al. (1995).

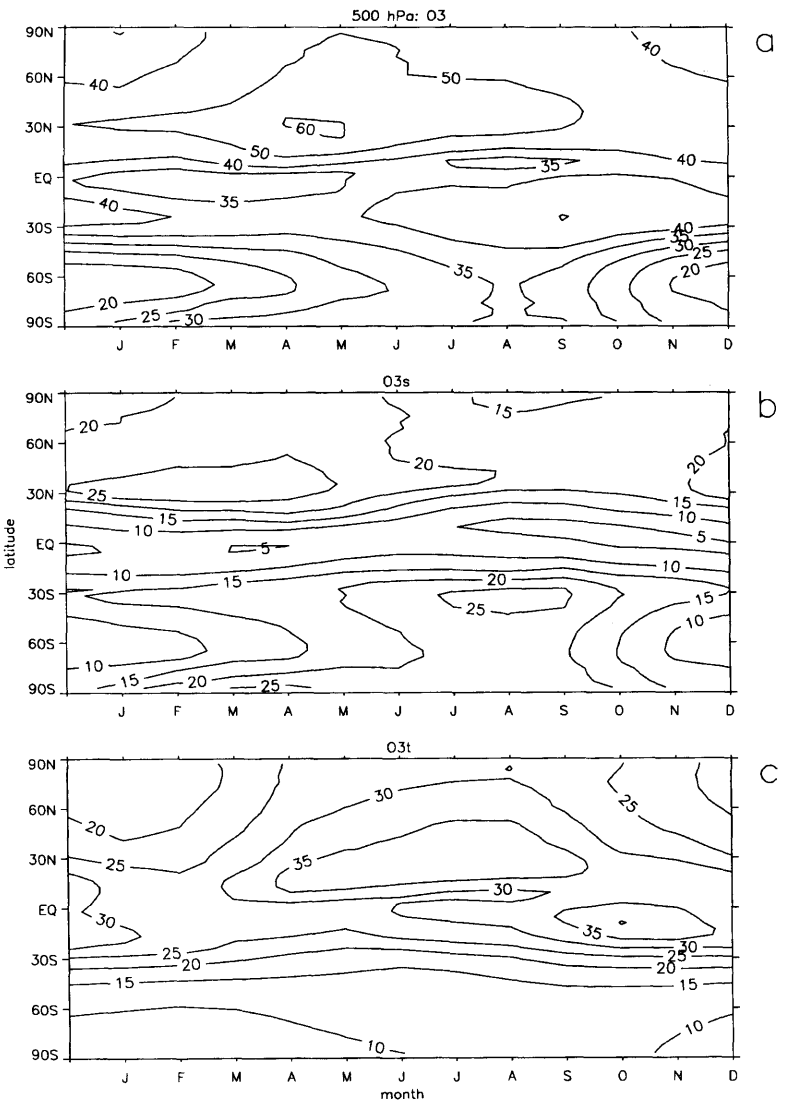

Fig. 4. As Fig. 3, but at 500 hPa.

In the Mace Head area O_3 peaks in spring, consistent with observations. The spring maximum appears to be the result of downward O_3 transport from the stratosphere as well as photochemical O_3 production in the troposphere. O_3s maximizes in February and March and decreases afterward due to the decreasing role of STE and increasing photochemical destruction. Since the Mace Head grid represents a relatively clean area with low local NO_x-emissions, photochemical O_3 is mainly transported to this region from more polluted areas. O_3 is lower in summer than in spring because photochemical destruction of O_3 prevails in NO_x-poor regions. Total O_3 increases again in the fall due to enhancement of STE and the increasing photochemical lifetime of O_3 compared to the summer.

For Mace Head and Payerne the O_3s seasonality is very similar. In Payerne, however, photochemical production of O_3 maximizes in summer.

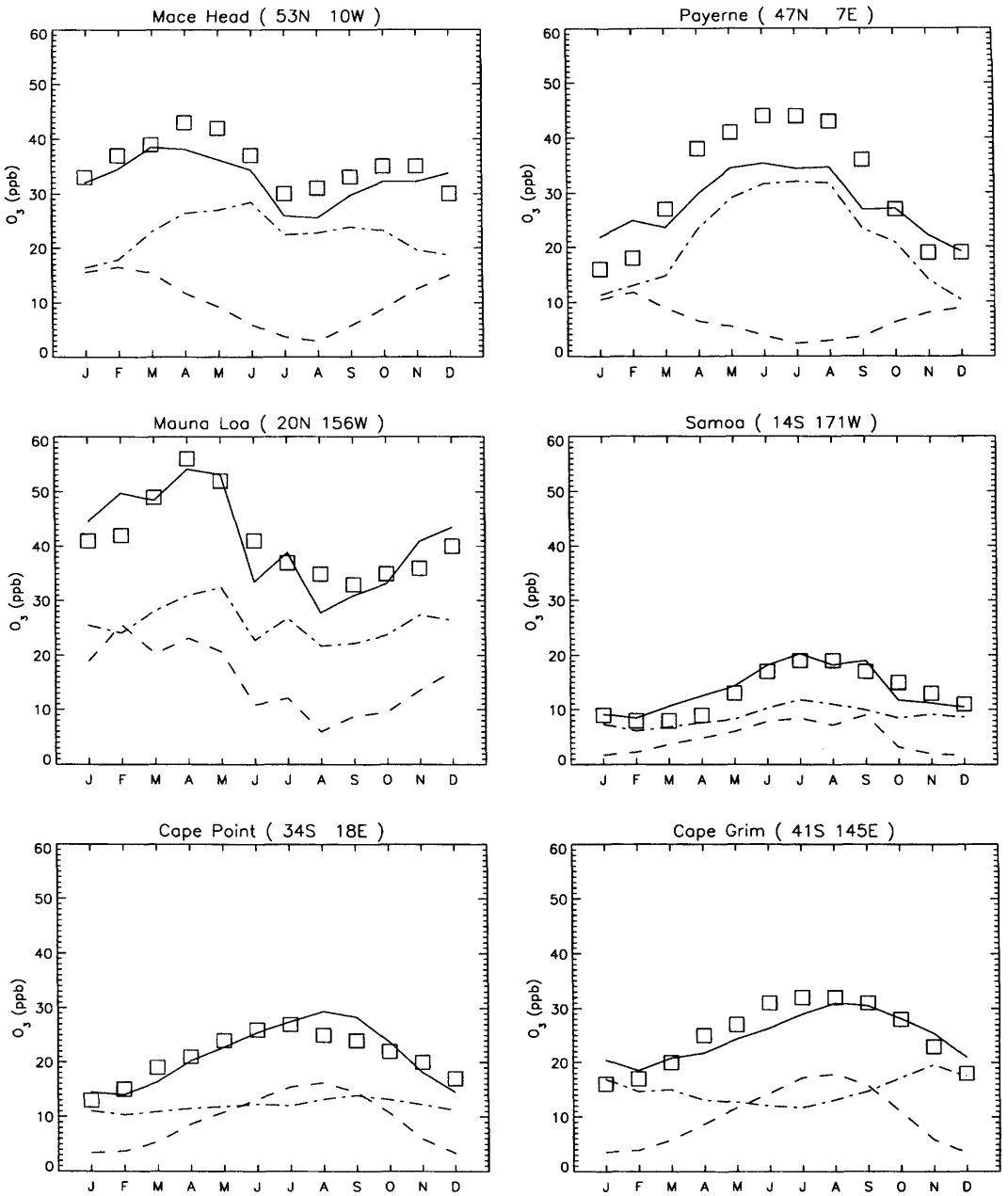

Fig. 5. Calculated monthly varying surface concentrations (ppbv) for total O_3 (solid line), O_3s (dashed line), and O_3t (dashed-dotted line) for grid cells representing (a) Western Ireland (Mace Head), (b) Central Europe (Payerne), (c) and (d) the tropical Pacific (Mauna Loa, Samoa), (e) Southern Africa (Cape Point), and (f) Tasmania (Cape Grim). Measurements, indicated by squares, have been obtained from Oltmans and Levy (1994) and the World Ozone Data Center.

A box model analysis of ozone soundings at Payerne gave rise to a similar conclusion (Austin and Follows, 1991). The STE and tropospheric O_3 contributions are, as in Mace Head, of comparable magnitude in winter. For Mauna Loa the model captures the observed spring O_3 peak relatively well. The seasonality at Mauna Loa appears to be mainly determined by that of O_3s, which is similar to that at more northern latitudes, but absolute concentrations are higher because of the height above sea level. Concentrations of O_3t are relatively high in late spring, partly as a result of relatively strong photochemical production, but also due to the relatively long lifetime of O_3 compared to the summer, which allows for significant transports from continental regions. In the three SH locations, O_3 has a winter maximum and a summer minimum. The seasonality of O_3 is dominated by the seasonality of O_3s, as O_3t varies only weakly.

Global seasonally dependent distributions of O_3, O_3s, and O_3t are given in Figs. 6 (DJF), 7 (MAM), 8 (JJA), and 9 (SON). The top panels show total O_3 from the surface to the tropopause (in Dobson units). These can be compared with tropospheric O_3 columns derived from the TOMS minus SAGE sattelite data set of Fishman et al. (1990). The calculated O_3 columns are in reasonable agreement with the Fishman et al. analysis for the SH tropics, with peak values over South America, Central Africa, and the Atlantic Ocean during SON, the biomass burning season. The O_3 low over the equatorial Pacific, reaching into the equatorial Indian Ocean, is represented well, with values down to 15 DU throughout the year. Calculated O_3 columns appear to be overestimated in DJF and MAM at 30° latitude in the NH, especially over northern Africa. Although it is possible that the model overestimates downward transport of O_3 from the stratosphere in these locations, it is important to realize that the tropopause height is a critical parameter in the calculation of tropospheric O_3 columns. The relatively coarse vertical resolution of the model around the tropopause, where O_3 concentrations are highest, may lead to significant discrepancies between model results and satellite retrieved O_3 columns. This may be especially important in the subtropics near the tropopause break where tropopause heights vary strongly with latitude. Of course, the same argument applies to the retrieval of O_3 columns from radiances observed by satellites. Satellite measurements of O_3 have recently gained accuracy by improved treatment of marine stratocumulus clouds and lower tropospheric ozone in TOMS retrieval algorithms (Hudson et al., 1995). Model calculated O_3 columns appear to be too low at higher latitudes, especially in the SH. Previous analysis has shown that the model underestimates tropospheric O_3 by up to a factor of 2 near the south pole (Roelofs and Lelieveld, 1995); this has not significantly improved in the present version. In the NH, the largest differences occur during the summer. Here, neglect of higher hydrocarbon chemistry in our model is expected to lead to an underestimation of O_3. Qualitatively, the O_3 maxima east of Asia, and in North America and Europe during spring and summer, correspond well with Fishman et al. (1990).

The middle panels in Figs. 6–9 show calculated O_3s columns. In general, O_3s column abundances are highest at about 30° latitude. They are lowest near the equator, where little downward transport through the tropopause occurs and chemical destruction prevails, and towards the poles, where the tropopause height and thus the tropospheric O_3 column is at minimum. In the NH winter and spring, O_3s is most abundant between 30 and 50° latitude, especially in subsidence areas over northern Africa and the Pacific, with O_3s columns exceeding 20 DU. In the SH, maximum O_3s columns of more than 20 DU occur in JJA.

In the tropics the contribution of stratospheric O_3 is relatively small and the photochemical production of O_3 predominates throughout the year, as can be seen in the lower panels of Figs. 6–9. The O_3 maximum during SON over the tropical Atlantic Ocean, as shown in Fig. 9c of Fishman et al. (1990), appears to be directly related to photochemical production from biomass burning emissions over Africa. Model results also suggest strong O_3 production north of the equator in Africa during MAM due to biomass burning. The O_3 produced from biomass burning emissions is transported efficiently over the tropical Atlantic Ocean, and during SON also over the southern Indian Ocean towards Australia. The equatorial Indian Ocean acts as a sink for O_3 during most of the year. Photochemical destruction of O_3 is efficient due to high water vapor concentrations and high insolation (reactions R7 and R8). Significant O_3 production also occurs in south-

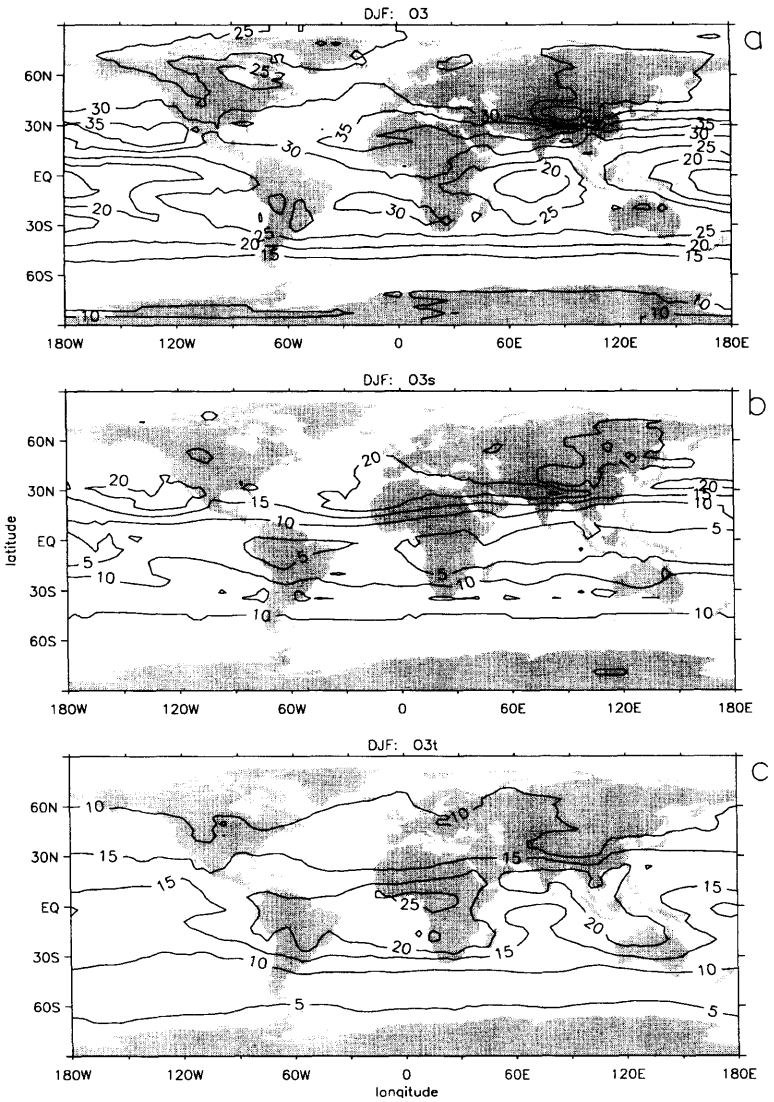

Fig. 6. Integrated tropospheric columns (Dobson units) of (a) total O_3, (b) O_3 originating from the stratosphere (O_3s), and (c) O_3 originating from photochemical production in the troposphere (O_3t), for DJF.

east Asia, especially during MAM and JJA. In middle and high northern latitudes, photochemical production of O_3 is important over most of the continents. In the NH summer months, O_3t columns exceed those of O_3s, but in the winter months, when photochemical production is least efficient and downward transport from the stratosphere is at maximum, the O_3s columns dominate.

4. Conclusions

We calculated that the net annual and global cross-tropopause flux of O_3 from the stratosphere into the troposphere is the result of a relatively large downward flux of stratospheric O_3, and a smaller upward flux of photochemically produced tropospheric O_3. Thus, the model simulates rela-

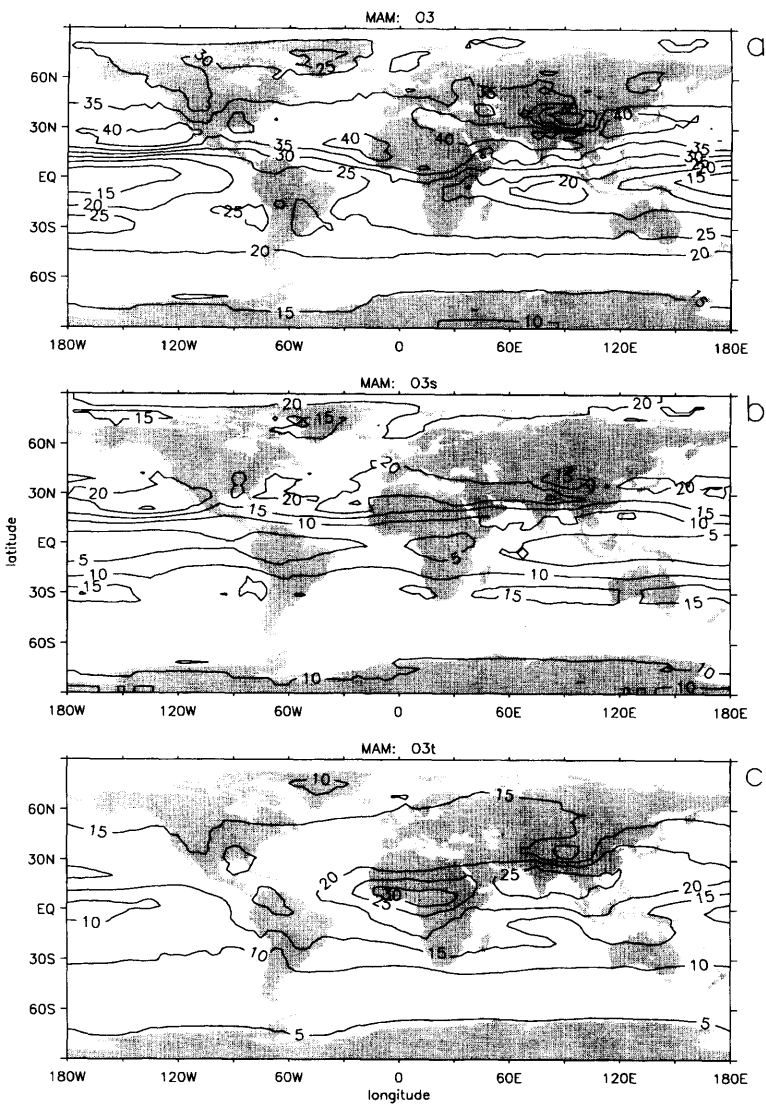

Fig. 7. As Fig. 6 but for MAM.

tively efficient two-way exchange between the upper troposphere and lower stratosphere at middle and high latitudes. This supports the concept of a lowermost stratosphere, where cross-tropopause transports take place along isentropic surfaces, being a transition region between the well mixed troposphere and the stable stratosphere (Holton et al., 1996). The calculated global net cross-tropopause flux of 459 Tg O_3 yr^{-1} is in accord with earlier estimates.

The model calculations suggest that stratospheric O_3, after transport through the tropopause, is mixed relatively efficiently throughout the troposphere. This is a consequence of the fact that most O_3 enters the troposphere in the winter and spring months, when O_3 lifetimes in middle and high latitudes are relatively long. On the other hand, much of the O_3 enters the troposphere in the subtropics where it is efficiently carried to the earth surface in the downward branches of the

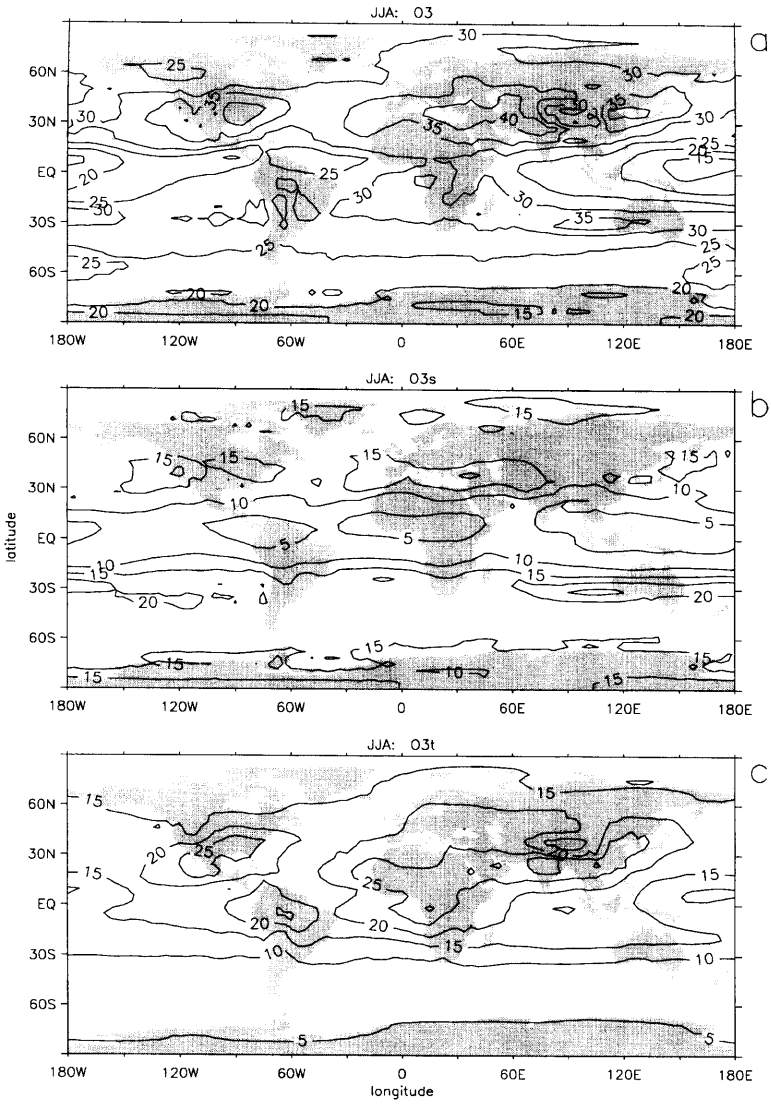

Fig. 8. As Fig. 6 but for JJA.

tropical Hadley cells. In the NH middle and high latitudes downward transport of O_3 rich air, associated with large-scale synoptical disturbances, appears efficient as well. At the surface, O_3 is rapidly destroyed by photochemistry, especially in the summer and at the equator, and by dry deposition. We find that O_3 originating from the stratosphere contributes on average 40% to O_3 in the troposphere. At the surface, this varies between about 10% in summer and at the equator, to 60% in winter. These values are much higher than those derived in previous stratospheric O_3 tracer studies (Follows and Austin, 1992), due to the more detailed treatment of transports across the tropopause and within the troposphere in our model.

Through the analysis of the residual between total O_3 and stratospheric O_3 we have assessed the contribution of O_3 that is photochemically produced from emissions in the troposphere. We calculate that roughly 55% of the surface O_3 in

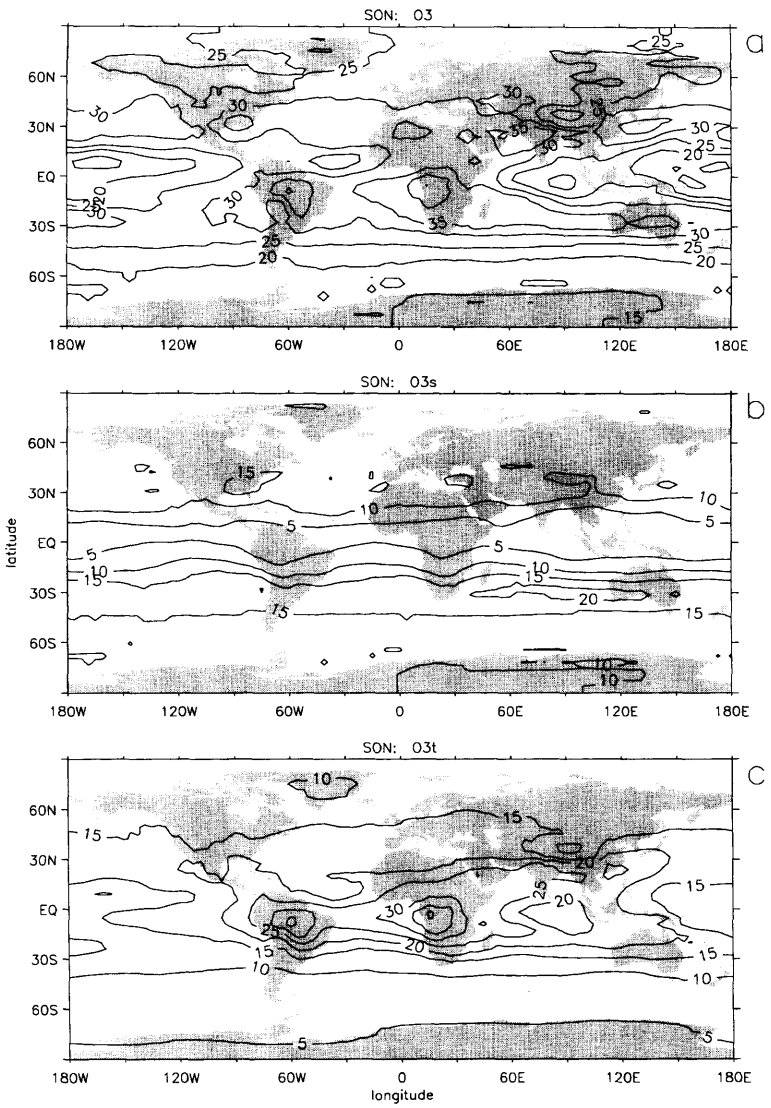

Fig. 9. As Fig. 6 but for SON.

the SH is determined by photochemical production in the troposphere, whereas in the NH this fraction is about 70%. Remarkably, these fractions in the mid-troposphere (500 hPa) are very similar. The ozone mixing ratios at 500 hPa are about 2 times higher compared to the surface, and the amounts of photochemically produced O_3 are quite high, up to 40 ppbv, in the NH summer. The absence of surface deposition and the relatively slow rate of O_3 destruction through reaction R8 in the dry free troposphere lead to a comparatively long lifetime of O_3. It is interesting to compare this with preliminary results of a simulation with pre-industrial emission estimates. These indicate a global mean contribution of photochemically produced O_3 to total O_3 of 50% at the surface, and NH summer mixing ratios at 500 hPa of about 20 ppb, approximately half of the calculated industrial O_3t levels. This confirms that anthropogenic emissions have caused a strong increase of tropo-

spheric O_3 levels (Crutzen and Zimmermann, 1991; Volz and Kley, 1988; Logan, 1994).

STE considerably influences the seasonality of surface O_3. In the extratropical SH, where practically no emissions of O_3-precursors occur, photochemically produced O_3 does not vary substantially with season, whereas O_3 from the stratosphere has a distinct winter maximum and summer minimum. In tropical regions, only a small amount of O_3 from the stratosphere reaches the surface, and the seasonality of surface O_3 is dominated by photochemical production in the troposphere. The influence of biomass burning emissions on O_3 production in the dry season is distinct over the tropical continents and the adjacent oceans, in particular over the Atlantic Ocean. These results agree well with O_3 distributions derived from satellite measurements (Fishman et al., 1990). Over the NH continents the seasonality of surface O_3 is determined mainly by photochemical production of O_3, with a maximum in summer and a minimum in winter. Stratospheric O_3 contributes significantly to tropospheric O_3 in winter. In relatively clean areas, e.g., over the north Atlantic Ocean, photochemically produced O_3 has a local minimum in summer because O_3 lifetimes are short. In these areas O_3 from the stratosphere contributes significantly throughout the year except in summer.

5. Acknowledgement

We thank the Max-Planck-Institute for Meteorology in Hamburg for the use of computer facilities and support, and Frank Dentener for discussions and comments on the manuscript. We also wish to thank Paul Fortuin for assistence with the retrieval of the WODC data. This work is part of the SINDICATE project, which is supported by the European Commission (D6-X11).

REFERENCES

Appenzeller, C., Davies, H. C. and Norton, W. A. 1996. Fragmentation of stratospheric intrusions. *J. Geophys. Res.* **101**, 1435–1456.

Austin, J. F. and Follows, M. J. 1991. The ozone record at Payerne: an assessment of the cross-tropopause flux. *Atmos. Environ.* **25A**, 1873–1880.

Benkovitz, C. M., Scholtz, M. T., Pacyna, J., Tarrason, L., Dignon, J., Voldner, E. C., Spiro, P. A., Logan, J. A. and Graedel, T. E. 1996. Global gridded inventories of anthropogenic emissions of sulfur and nitrogen, *J. Geophys. Res.*, in press.

Boer, G. J., Arpe, K., Blackburn, M., Déqué, M., Gates, W. L., Hart, T. L., le Treut, H., Roeckner, E., Sheinin, D. A., Simmonds, I., Smith, R. N. B., Tokioka, T., Wetherald, R. T. and Williamson, D. 1992. Some results from an intercomparison of the climates simulated by 14 atmospheric general circulation models. *J. Geophys. Res.* **97**, 12771–12786.

Brost, R. A., Feichter, J. and Heimann M. 1991. Three-dimensional simulation of ^{7}Be in a global climate model. *J. Geophys. Res.* **96**, 22423–22445.

Brühl, C., and Crutzen, P. J. 1988. Scenarios of possible changes in atmospheric temperatures and ozone concentrations due to man's activities, estimated with a one-dimensional coupled photochemical climate model. *Climate Dynamics* **2**, 173–203.

Crutzen, P. J. 1995. Ozone in the troposphere. In: *Composition, chemistry, and climate of the atmosphere* (ed. H. B. Singh). Van Nostrand Reinold Publ., New York, 349–393.

Crutzen, P. J. and Zimmermann, P. H. 1991. The changing photochemistry of the troposphere. *Tellus* **43A/B**, 136–151.

Danielsen, E. F. 1968. Stratospheric-tropospheric exchange based on radio-activity, ozone and potential vorticity. *J. Atmos. Sci.* **25**, 502–518.

Danielsen, E. F. and Mohnen, V. A. 1977. Project Dustorm report: Ozone transport, in situ measurements and meteorological analyses of tropopause folding. *J. Geophys. Res.* **82**, 5867–5877.

Dentener, F., Hein, R. and Roelofs, G. J. 1995. A comparison of background ozone concentrations calculated by the three dimensional models ECHAM, MOGUNTIA and TM2 with measurements. *Report CM-88.* Department of Meteorology, Stockholm University, Sweden.

Ebel, A., Elbern, H. and Oberreuter, A. 1993. Stratosphere-troposphere air mass exchange and cross-tropopause fluxes of ozone. In: *Coupling processes in the lower and middle atmosphere* (ed. E. V. Thrane). Kluwer, Dordrecht, 49–65.

Feichter, J., Brost, R. A. and Heimann, M. 1991. Three-dimensional modeling of the concentration and deposition of ^{210}Pb aerosols. *J. Geophys. Res.* **96**, 22447–22460.

Feichter, J., Kjellström, E., Rodhe, H., Dentener, F., Lelieveld, J. and Roelofs, G. J. 1996. Simulation of the tropospheric sulfur cycle in a global climate model. *Atmos. Environ.*, **30**, 1693–1707.

Fishman, J., Ramanathan, V., Crutzen, P. J. and Liu, S. C. 1979. Tropospheric ozone and climate. *Nature* **282**, 818–820.

Fishman, J., Watson, C. E., Larsen, J. C. and Logan, J. A. 1990. Distribution of tropospheric ozone determined from satellite data. *J. Geophys. Res.* **95**, 3599–3617.

Follows, M. J. and Austin, J. F. 1992. A zonal average model of the stratospheric contributions to the tropospheric ozone budget. *J. Geophys. Res.* **97**, 18047–18060.

Ganzeveld, L. and Lelieveld, J. 1995. Dry deposition parameterization in a chemistry general circulation model and its influence on the distribution of reactive trace gases. *J. Geophys. Res.* **100**, 20999–21012.

Gidel, L. T. and Shapiro, M. A. 1980. General circulation model estimates of the net vertical flux of ozone in the lower stratosphere and the implications for the tropospheric ozone budget. *J. Geophys. Res.* **85**, 4049–4058.

Hao, W. M. and Liu, M. H. 1994. Spatial and temporal distribution of tropical biomass burning. *Global Biogeochem. Cycles* **8**, 495–503.

Haskins, R. D., Barnett, T. P., Tyree, M. M. and Roeckner, E. 1995. Comparison of cloud fields from atmospheric general circulation model, in situ and satellite measurements. *J. Geophys. Res.* **100**, 1367–1378.

Hoerling, M. P., Schaack, T. K. and Lenzen, A. J. 1993. A global analysis of stratospheric-tropospheric exchange during northern winter. *Mon. Wea. Rev.* **121**, 162–172.

Holton, J. R., Haynes, P. H., McIntyre, M. E., Douglas, A. R., Rood, R. B. and Pfister, L. 1996. Stratosphere-troposphere exchange. *Reviews of Geophysics*, **33**, 403–409.

Holton, J. R. and Lelieveld, J. 1996. Stratosphere-troposphere exchange and its role in the budget of tropospheric ozone. In: *Clouds, chemistry and climate* (ed. P. J. Crutzen and V. Ramanathan). NATO ASI Series, Springer-Verlag, Berlin, 173–190.

Hudson, R. D., Kim, J. H. and Thompson, A. M. 1995. On the derivation of tropospheric column ozone from radiances measured by the total ozone mapping spectrometer. *J. Geophys. Res.* **100**, 11137–11145.

Levy II, H., Mahlman, J. D., Moxim, W. J. and Liu, S. C. 1985. Tropospheric ozone: The role of transport. *J. Geophys. Res.* **90**, 3753–3772.

Logan, J. A. 1994. Trends in the vertical distribution of ozone. An analysis of ozonesonde data. *J. Geophys. Res.* **99**, 25553–25585.

Mahlman, J. D., Levy II, H. and Moxim, W. J. 1980. Three-dimensional tracer structure and behaviour as simulated in two ozone-precursor experiments. *J. Atm. Sci.* **37**, 655–685.

Murphy, D. M. and Fahey, D. W. 1994. An estimate of the flux of stratospheric reactive nitrogen and ozone into the troposphere. *J. Geophys. Res.* **99**, 5325–5332.

Oltmans, S. J. and Levy II, H. 1994. Surface ozone measurements from a global network. *Atmos. Environ.* **28**, 9–24.

Price, C. and Rind, D. 1992. A simple lightning parameterization for calculating global lightning distributions. *J. Geophys. Res.* **97**, 9919–9933.

Ramanathan, V., Callis, L., Cess, R., Hansen, J., Isaksen, I., Kuhn, W., Lacis, A., Luther, F., Mahlman, J., Reck, R. and Schlesinger, M. 1987. Climate-chemical interactions and effects of changing atmospheric trace gases. *Rev. Geophys.* **25**, 1441–1482.

Rasch, P. J. and Williamson, D. 1990. Computational aspects of moisture transport in global models of the atmosphere. *Q. J. R. Meteorol. Soc.* **116**, 1071–1090.

Roeckner, E., Arpe, K., Bengtsson, L., Brinkop, S., Dümenil, L., Esch, M., Kirk, E., Lunkeit, F., Ponater, M., Rockel, B., Sausen, R., Schlese, U., Schubert, S. and Windelband, M. 1992. Simulation of the present-day climate with the ECHAM model: Impact of model physics and resolution. *Report no.* **93**. Max-Planck-Institute for Meteorology, Hamburg, Germany.

Roeckner, E., Siebert, T. and Feichter, J. 1995. Climatic response to anthropogenic sulfate forcing simulated with a general circulation model. In: *Aerosol forcing of climate* (ed. R. J. Charlson and J. Heintzenberg). John Wiley and Sons, New York, pp. 349–362.

Roelofs, G. J. and Lelieveld, J. 1995. Distribution and budget of O_3 in the troposphere calculated with a chemistry — general circulation model. *J. Geophys. Res.* **100**, 20983–20998.

Tiedtke, M. 1989. A comprehensive mass flux scheme for cumulus parameterization in large-scale models. *Mon. Wea. Rev.* **117**, 1779–1800.

Vaughan, G. 1988. Stratosphere-troposphere exchange of ozone. In: *Tropospheric ozone* (ed. I. S. A. Isaksen). D. Reidel, Dordrecht, pp. 125–135.

Volz, A. and Kley, D. 1988. Evaluation of the Montsouris series of ozone measurements made in the nineteenth century. *Nature* **332**, 240–242.

World Meteorological Organization 1995. *Scientific assessment of depletion: 1994*, Global ozone research and monitoring project, *Report* **37**. Geneva, Switzerland.

Yienger, J. J. and Levy II, H. 1995. Empirical model of global soil-biogenic NO_x emissions. *J. Geophys. Res.* **100**, 11447–11464.